Image effects on direct and inverse photoemission of CO adsorbed on NiAl(110)

1992 J. Phys.: Condens. Matter 4 5103

(http://iopscience.iop.org/0953-8984/4/22/010)

J. Phys.: Condens. Matter 4 (1992) 5103–5124. Printed in the UK

Image effects on direct and inverse photoemission of CO adsorbed on NiAl(110)

Maria Elena Grillo, German R Castro†, and Gerold Doyen

Fritz-Haber-Institut der MPG, Faradayweg 4-6, D-W1000 Berlin 33, Federal Republic of Germany

Received 7 January 1992

Abstract. The aim of this investigation is to elucidate the nature of the direct and inverse photoemission behaviour of CO adsorbed on NiAl(110). ARUPS reveals that the CO-5σ-derived ionization energy on NiAl(110) is surprisingly large in view of the moderate adsorption energy. A dynamical image theory explains the large 5σ ionization energy. The general shape of the theoretical electron–hole excitation spectrum is in accordance with the experimental direct and inverse photoemission spectra. The splitting of the 2π-derived features in the inverse photoemission spectrum is explained by the theory as well. CO adsorption on NiAl(110) is studied by means of a model Hamiltonian which includes electron correlation effects in the environment of the adsorbed molecule and image effects as a coupling of the adsorbate electrons to the surface plasmons. The coupling constants for the adsorbate–plasmon interaction are calculated from first principles. The charge density describing the image screening by the surface plasmons is calculated self-consistently. The electron–hole excitation energies are obtained as differences between the self-consistent (negative and positive) ionized states and the ground state.

1. Introduction

The image energy plays an important role in stabilizing an adsorbate on a metal surface. In particular its importance for alkali adsorption on simple and transition metals has been recognized. Recent theoretical studies have focussed on two different microscopic mechanisms for the origin of image charge effects. First there are the theories dealing with the response of metal surface electrons to the perturbing electric field of an external static charge (Lang and Kohn 1973, Kahn and Ying 1976, Russier and Mijoule 1991). An early calculation determined the image plane position as a function of the distance of the static charge from a jellium surface (Appelbaum and Hamann 1972).

In the second approach the screening surface charge density due to the long-range interaction with the adsorbate is decomposed into a sum of coherently displaced surface plasmons. In this description (Sunjic *et al* 1972) the image potential arises from the polarization of the plasmons by the adatom charges. The importance of the surface plasmon excitation for the image potential has been emphasized before (Lucas 1971, Mahan 1972, Ritchie 1972). In addition it was found that van der Waals forces also have their origin in the polarization of these surfaces modes (Gerlach 1971).

† Permanent address: Institut für Physikalische Chemie, Universität Bonn, Federal Republic of Germany.

0953-8984/92/225103+22$04.50

Several attempts have been made to introduce the image interaction or non-local correlation effects in chemisorption models. In early work the interaction of a metallic surface with an adsorbed alkali atom was represented by the classical image potential (cf for example the perturbation approach (Gadzuk 1967, Remy 1970)). In other investigations the non-local effects are included via a renormalization of the gas atom parameters. This point of view was also adopted by Doyen and co-workers in a model Hamiltonian approach to adsorption which, in the remainder of this article, is referred to as MOHAAD (Drakova *et al* 1985, Drakova *et al* 1988). Here the core energies and the Coulomb interactions are renormalized consistently with the correct adiabatic limit of the image energy (Hewson and Newns 1974). The image potential used in MOHAAD to renormalize the adatom parameters is that calculated by Appelbaum and Hamann for a static point charge near a metal surface (Appelbaum and Hamann 1972). A similar renormalization of the gas atom parameters has been used before (Anda *et al* 1977) in the framework of the Anderson Hamiltonian.

The first dynamic treatment of the the image interaction for adsorbates was developed by Hewson and Newns based on the Anderson Hamiltonian but neglecting electron–electron repulsion of the adatom (Hewson and Newns 1974). The idea was to consider the image interaction as a coupling of the adatom to the surface plasmons. This extension of the Anderson formalism is referred to as the extended Anderson Hamiltonian (EAH). Hewson and Newns restricted their treatment to the study of systems such as alkali atoms adsorbed on transition metal surfaces for which they ignore both spin and Coulomb interaction on the adatom. Some years later Anda and Ure using the same ideas developed a theory of hydrogen chemisorption, which included spin dependence and electronic repulsion of the adsorbate (Anda and Ure 1979). Numerical results were obtained for hydrogen adsorbed on tungsten explaining the peaks observed in photoemission experiments. Within the EAH model the effect of adsorbate charge fluctuations on the ionic part of the chemisorption energy was also investigated (Braun and Volokitin 1983). In this work the exact solution for a one-electron two-level model as well as a variational solution for the EAH model was reported.

Cini proposed a quantum mechanical theory for the photoemission spectrum of a surface molecule interacting with the surface plasmon field within the EAH model (Cini 1978, 1979). The electron–surface plasmon coupling includes not only the plasmon screening of the adsorbate electrons (image effect), but also the polarization term due to the plasmons that cause transitions between the adatom orbitals and the metal states, whereas image-induced transitions between adorbitals are neglected. An effective charge–plasmon coupling constant was calculated using the hydrodynamic model (Ritchie and Wilems 1969) for the special case where the adsorbate metal polarization term is small compared to the adsorbate–image force coupling. In the hydrodynamic model the plasmon wave vector is integrated up to infinity overestimating all polarization effects in absolute magnitude. The results for inert gases or other closed shell species interacting with a transition metal surface imply an adsorption mechanism due to both plasmon and adsorbate polarization.

The theory of image force surface plasmon polarization was also used to study the relaxation shift experienced by different adorbital hole states of a given adsorbed molecule (Gadzuk 1976, 1977, Gadzuk and Doniach 1978) and has been applied to the problem of valence level photoemission from CO adsorbed on semi-infinite jellium (Dunlap and Gadzuk 1980). In particular, the dependence of the relaxation shifts on molecular orbital shape and position relative to the surface was investigated.

Image potential shifts in the 1–2 V range were obtained varying by a few tenths of an eV depending upon which orbital was ionized. The image potential shifts were found to be rather independent of the shape and transverse extent of the adorbitals, but strongly dependent on the centre of charge. A serious limitation in the applicability of this theory is that the hole must be totally outside the surface.

In the present investigation the image charge effect is described by the interaction of the adatom with the surface plasmons. Our work differs from previous studies in that

(1) the coupling constants for the adsorbate–plasmon interaction are calculated from first principles avoiding the hydrodynamic limit;
(2) the polarization of the adparticle due to the plasmon interaction is included;
(3) the electron correlation in the environment of the adparticle is included and the charge density is calculated self-consistently in the presence of the plasmon coupling.

The dynamic image interaction is obtained by solving self-consistently for the interacting electron–plasmon system. Hence, the image energy depends on the dynamic screening charge, which varies with the adsorption site. In this way we may attempt to describe a corrugation in the image potential parallel to the surface. This work represents an extension of MOHAAD, which includes the image effects in a dynamic way. MOHAAD, which has been described before in detail (Doyen 1976, 1977, Drakova *et al* 1985, 1988), has been successfully applied to adsorption on simple and transition metals.

Table 1. CO-derived ionizaton energies in eV relative to the Fermi level for CO adsorbed on NiAl(110).

CO orbital	SCF static	SCF dynamic	Experiment
4σ	11.72	11.94	11.7
1π	9.02	9.21	7.9
5σ	7.67	8.76	8.9
2π	− 1.72	− 1.73	− 2.0
	− 5.99	− 6.36	− 4.6
Reference	Grillo *et al* (1992)		Isern (1990)

The theory, which is described in detail in section 2, is used to calculate the electron–hole excitation spectrum of CO adsorbed on NiAl(110). This spectrum is surprisingly different to the one obtained for CO adsorbed on Cu in view of the similar electronic structures of Cu and NiAl (Mundenar *et al* 1987, Isern 1990) as well as the similar adsorption energies of CO on the two metals. ARUPS reveals a strong downward shift of the 5σ ionization energy for CO on NiAl(110) (cf table 1 and section 3.3.1). The aim of the present work is to understand the inverse and direct photoemission spectra of CO adsorbed on NiAl(110).

In the present dynamic approach two different mechanisms are included in the calculated relaxation shifts experienced by the different molecular orbital hole states on the CO molecule. These are the virtual excitations of surface plasmons (*non-local adsorbate–substrate interaction*) and the adsorbate–substrate interference (*local interaction*). In section 3.4 we compare the relative contributions of these two mechanisms for the relaxation shifts of the different CO-induced orbital hole states on NiAl(110)

at the equilibrium position. The different magnitudes of the relaxation shifts for different CO-induced chemisorption orbitals are discussed as well.

2. Theoretical formalism

In this section we describe the extension of MOHAAD to include the interaction of the adsorbate charges with the surface plasmons. The changes in the surface density due to the long-range interaction with the adsorbate are described by means of the collective charge oscillations of the electron gas. We consider here degenerate plasmons as the quantized charge oscillations. The total interaction of the adsorbate with the metal surface is described by the Hamiltonian

$$H = H_{\text{loc}} + H_{\text{p}}$$

where H_{loc} describes the interaction in the surface molecule region and

$$H_{\text{p}} = \omega_{\text{p}} \sum_k b_k^+ b_k + \sum_{i,j,k} \lambda_k^{ij} a_i^+ a_j (b_k^+ + b_k) + \sum_{k,N} \lambda_k^N (b_k + b_k^+) \quad (1)$$

contains the interaction with the surface plasmons. b_k^+ and b_k represent plasmon creation and annihilation operators. ω_{p} is the surface plasmon frequency. a_i^+ and a_j are electron creation and annihilation operators. λ_k^{ij} and λ_k^N are the coupling constants to the kth plasmon mode of the electron charge $\rho_{ij} = \phi_i^* \phi_j$ and the adsorbate nucleus, respectively. The first term in H_{p} describes non-dispersive plasmons with energy-independent wave numbers. The last two terms in H_{p} describe the interaction between the plasmons and the adsorbate.

2.1. Adsorbate-projected local plasmons

If we consider non-dispersive plasmons we can construct adsorbate-projected local plasmon modes by means of the following transformation:

$$\alpha_{ij} = \frac{1}{B_{ij}} \sum_k \lambda_k^{ij} b_k \quad (2)$$

$$\alpha_N = \frac{1}{B_N} \sum_k \lambda_k^N b_k. \quad (3)$$

α_{ij} is the transformed plasmon mode projected on the adsorbate charge distribution $\rho_{ij} = \psi_i^* \psi_j$ and α_N is the mode projected on the adcore charge Q_N. B_{ij} and B_N are normalization constants

$$B_{ij} = \sqrt{\sum_k |\lambda_k^{ij}|^2} \qquad B_N = \sqrt{\sum_k |\lambda_k^N|^2} \quad (4)$$

which have the physical meaning of coupling constants. The transformed plasmon modes have the maximum coupling to the adsorbate charges. The adsorbate-projected

plasmons are non-orthogonal to the non-local plasmon modes b_k with overlap integrals defined by:

$$S_{ijk} = \langle \alpha_{ij} \mid b_k \rangle = \frac{\lambda_k^{ij}}{B_{ij}}.$$

The non-local plasmon modes b_k are now orthogonalized to the new local modes α_{ij}, so

$$\langle \alpha_{ij} \mid \tilde{b}_k \rangle = 0.$$

It can be shown that these new modes $\tilde{b}_k$ decouple exactly and only the new adsorbate-projected modes appear in the plasmon-coupling term. Thus the plasmon operator can be rewritten in the form:

$$\tilde{H}_p = \omega_p \left(\sum_{ij} \alpha_{ij}^+ \alpha_{ij} + \sum_N \alpha_N^+ \alpha_N + \sum_k \tilde{b}_k^+ \tilde{b}_k \right) + H_{ep}$$

with

$$H_{ep} = \sum_{ij} B_{ij} a_i^+ a_j (\alpha_{ij}^+ + \alpha_{ij}) + \sum_N B_N (\alpha_N^+ + \alpha_N). \tag{5}$$

The new localized basis of the adsorbate-projected plasmons reduces the dimension of the problem. Instead of coupling to a large number of delocalized plasmon modes one has coupling only to a limited number of modes. The transformed Hamiltonian contains solely the interaction of the adsorbate with the projected modes. For the sake of briefness we introduce the following compact notation:

$$D_{ij} = B_{ij} a_i^+ a_j$$
$$D_N = B_N.$$

D_{ij} is a one-electron operator and D_N is a c-number. From now on we introduce a matrix notation by arranging these quantities and the projected plasmons modes as *column vectors* $\boldsymbol{D}$ *and* $\boldsymbol{\alpha}$, *respectively*. The plasmon coupling can then be written in vector notation

$$H_{ep} = \boldsymbol{D}^T \cdot (\boldsymbol{\alpha} + \boldsymbol{\alpha}^+) \tag{6}$$

where $\boldsymbol{D}^T$ denotes a row vector. The adsorbate projected plasmon modes are normalized but mutually non-orthogonal with overlap matrix elements

$$S_{ij,kl} = \langle \alpha_{ij} \mid \alpha_{kl} \rangle = \frac{1}{B_{ij} B_{kl}} \sum \lambda_k^{ij} \lambda_k^{kl}.$$

The coupling constants λ_k^{ij} are real numbers, so $(\lambda_k^{ij})^* = \lambda_k^{ij}$. An orthonormal set of plasmon operators can be created by means of symmetric orthogonalization (Löwdin 1950):

$$\tilde{\boldsymbol{\alpha}} = \mathbf{S}^{-1/2} \boldsymbol{\alpha}.$$

Inserting the orthogonal modes in the plasmon coupling yields

$$H_p = \omega_p \tilde{\boldsymbol{\alpha}}^+ \cdot \tilde{\boldsymbol{\alpha}} + H_{ep} + \text{decoupled modes}$$
$$H_{ep} = \boldsymbol{D}^T \cdot \mathbf{S}^{1/2} (\tilde{\boldsymbol{\alpha}}^+ + \tilde{\boldsymbol{\alpha}}).$$

2.2. Self-consistent solution of the plasmon coupling

The electron–plasmon interaction can approximately be removed by making the self-consistent canonical transformation

$$P = \tilde{\alpha} + \mathbf{S}^{1/2}\langle D\rangle/\omega_p. \tag{7}$$

$\langle D_{ij}\rangle$ is here the ground state expectation value of the electron operator D_{ij}. The self-consistent version of the Hamiltonian H_p^{SCF} transforms into

$$H_p^{SCF} = H_{po}^{SCF} + H_{ep}^{SCF} + (\text{decoupled modes})$$

where

$$H_{po}^{SCF} = \omega_p \sum_{m,n} (P_{mn}^{+} P_{mn})$$

and

$$H_{ep}^{SCF} = -\frac{2}{\omega_p} \boldsymbol{D}^{\top}\mathbf{S}\langle \boldsymbol{D}\rangle + \frac{1}{\omega_p}\langle \boldsymbol{D}\rangle^{\top}\mathbf{S}\langle \boldsymbol{D}\rangle.$$

In this equation, the electron–plasmon coupling has vanished, but the electron motion has been modified. H_{po}^{SCF} indicates decoupled shifted plasmon modes, the second term in H_{ep}^{SCF} is a constant shift of the potential. Of special interest is the first term in H_{ep}^{SCF} which shows that all one- and two-electron integrals are renormalized by the plasmon coupling in a self-consistent approximation. To see this, observe that the quadratic form $\boldsymbol{D}^{\top}\mathbf{S}\boldsymbol{D}$ is a sum of one- and two-electron operators:

$$-\frac{2}{\omega_p}\left(\sum_{ijmn} B_{ij} S_{ijmn} B_{mn} a_i^{+} a_j a_m^{+} a_n + \sum_{ijN} B_{ij} S_{ijN} B_N a_i^{+} a_j\right).$$

Here i, j, m, n run over the adorbitals and N over the adcores. $S_{ij,N} = \langle \alpha_k^{ij} \mid \alpha_N\rangle$ is the overlap integral between an adsorbate-projected plasmon α_{ij} and an adcore projected plasmon α_N. Physically this renormalization means that we do not have bare electrons, but electrons dressed in plasmon clouds.

The analytic evaluation of the coupling constants (cf section 2.4) reveals that at large distances from the surface the plasmon coupling just yields the classical image interaction. At shorter distances the divergency of the classical image force is avoided, because plasmons exist only for long wavelengths. At short wavelengths they merge into the continuum of electron–hole pair excitations.

Applying the formalism described to a neutral atom interacting with the surface plasmons yields at large distances from the surface just the classical limit for the Van der Waals interaction (Grillo 1991). To see the origin of the Van der Waals forces between an adsorbate and a solid surface it is important to consider the long-range adsorbate–metal surface interaction, which in our model is just the coupling to the plasmons. It arises from the polarization of the adsorbate electrons in response to the induced dipoles in the metal; hence it is the interaction of the polarizable solid with dipolar quantum mechanical fluctuations of the atomic charge distribution.

2.3. Comparison with the static approach

In this section we compare the new plasmon Hamiltonian formalism with the earlier version of MOHAAD (Drakova *et al* 1985), which included a static treatment of the image charge effects. In the dynamic approach the self-interaction of an electron in the ith adorbital has the form

$$V_{\text{self}} = (-2/\omega_p)\Big\{\Big(B_{ii}\langle n_i\rangle + \sum_j B_{ij}S_{ii,ij}\langle a_i^+ a_j\rangle + \sum_j B_{ji}S_{ii,ji}\langle a_j^+ a_i\rangle\Big)B_{ii}n_i$$
$$+ \sum_j \big[\big(B_{ii}S_{ij,ii}\langle n_i\rangle + B_{ij}\langle a_i^+ a_j\rangle + B_{ji}S_{ij,ji}\langle a_j^+ a_i\rangle\big)B_{ij}a_i^+ a_j$$
$$+ \big(B_{ii}S_{ji,ii}\langle n_i\rangle + B_{ij}S_{ji,ij}\langle a_i^+ a_j\rangle + B_{ji}\langle a_j^+ a_i\rangle\big)B_{ji}a_j^+ a_i\big]\Big\}$$
$$+ \text{expectation values corresponding to the last term of } H_{\text{ep}}^{\text{SCF}}.$$

Consider an adatom with a single occupied adorbital and an adcore of charge Q. This adatom has no overlap or charge exchange with the metal wave functions, but interacts only with the plasmon field. Therefore we have $\langle n_i\rangle = 1$ and $\langle a_i^+ a_j\rangle = 0$ in the ground state. In this limit the self-interaction reduces to

$$V_{\text{self}} = -2\frac{B_{ii}^2}{\omega_p}(n_i - \tfrac{1}{2}).$$

At large distances where this description is valid the adorbital and the adcore have the same image potential per unit charge, so $B_{ii}^2 = B_N^2/Q^2$ and therefore $S_{ii,N} = 1$. Adding the repulsion of the adelectrons from the adcore image $-2(B_{ii}B_N/\omega_p)n_i$ one obtains with $B_Q = -B_N$ the following renormalization of the adelectron ionization energy E_i:

$$E_i = E_i + \frac{B_{ii}^2}{\omega_p}\left(2\frac{B_Q}{B_{ii}} - 1\right).$$

The quantity $-B_{ii}^2/\omega_p$ is the attractive potential due to the interaction of the electron with its own image. Because $-B_Q^2/\omega_p$ is the potential corresponding to the image interaction of the core charge Q with itself, the ratio B_Q/B_{ii} is seen to be in this limit equal to the core charge Q.

In an analogous manner one obtains for the Coulomb interaction U_{ii} in the adorbital $|\,i\rangle$:

$$U_{ii} = U_{ii} - \frac{2}{\omega_p}B_{ii}^2.$$

In this way the static renormalization used before in the earlier approach to the image interaction can be identified (Drakova *et al* 1985).

In the static approach to the electron–hole excitation spectrum (Grillo *et al* 1992) the image effects appear in the initial state, whereas in the dynamic approach they show up in the final state (cf section 3.4). In the dynamic calculation the self-energy terms are calculated self-consistently and therefore depend on the self-consistent

charge density describing the image screening. Therefore the initial state one-electron energies are not renormalized with the electron self-image, which leads to more negative one-electron energies as compared to the static approach.

As an important consequence of this new method, the image potential effects are not included in the Koopmans' ionizations energies, whereas the ΔSCF ionization energies contain the full image relaxation effects of the final ion. This permits us to investigate the role of the long-range interaction in the relaxation process of the ionized state (cf section 3.4). This type of relaxation mechanism may be important in future work to explain some features in photoemission experiments of adsorbed surfaces such as satellite peaks.

2.4. Evaluation of the electron–plasmon coupling

To evaluated the adsorbate–plasmon coupling constant the interaction between the adsorbate electrons and the adsorbate-induced dipoles in the metal has to be considered. From classical electrodynamics the charge–dipole interaction potential for an electron at position (r_e, z_e) and a dipole at (r, z) with dipole moment μ can be written as

$$V^{\mathrm{dip}}(r, z) = \frac{(r, z + z_e) \cdot \mu}{[r^2 + (z + z_e)^2]^{3/2}}. \tag{8}$$

Here r_e and r are the coordinates of the electron and the dipole parallel to the surface plane, respectively. z_e and z are the coordinates perpendicular to the surface. The dipole–charge interaction is Fourier analysed as follows:

$$V^{\mathrm{dip}}(r, z) = \int \mathrm{d}k\, f(k, z) \mathrm{e}^{\mathrm{i}k \cdot r}.$$

The function $f(k, z)$ is the integral transform and is given by

$$f(k, z) = \frac{1}{\sqrt{2\pi}} \int_{-\infty}^{\infty} \mathrm{d}r\, \mathrm{e}^{-\mathrm{i}k \cdot r} f(r, z).$$

Substituting the result of this integral in the Fourier expansion for $V^{\mathrm{dip}}(r, z)$ one obtains:

$$V^{\mathrm{dip}}(r, z) = \int \mathrm{d}k\, f(k, z) \mathrm{e}^{\mathrm{i}k \cdot r} = \frac{A}{\sqrt{2\pi}} \int \mathrm{d}k\, \mathrm{e}^{-k|z + z_e|} \mathrm{e}^{\mathrm{i}k \cdot r}.$$

In order to evaluate the interaction energy with an electronic charge distribution on the adsorbate, the interaction potential $V^{\mathrm{dip}}(r, z)$ has to be integrated over the coordinates of the adsorbate electrons:

$$\lambda_k^{ij} = (A/2\pi)^{1/2} \int_{-\infty}^{\infty} \mathrm{d}^2 r_e \int_0^{\infty} \mathrm{d}z_e\, \psi_i^*(r_e, z_e) \psi_j(r_e, z_e) \mathrm{e}^{\mathrm{i}k \cdot r_e} \mathrm{e}^{-k|z + z_e|}. \tag{9}$$

Here λ_k^{ij} is the coupling constant in the Hamilton operator for the electron–plasmon interaction and $\psi_j(r_e, z_e)$ is an adsorbate wave function. The image potential of the adsorbate charge distribution ρ_{ij} is obtained by using the self-consistent canonical transformation equation (7):

$$V_{ij} = \frac{B_{ij}^2}{\omega_p} = \frac{\sum_k |\lambda_k^{ij}|^2}{\omega_p}. \tag{10}$$

Therefore the following integral has to be evaluated:

$$V_{ij}(\boldsymbol{r}_e, z_e) = \frac{A^2}{\omega_p 2\pi} \int_0^{K_c} dk_x \int_0^{K_c} dk_y \int_0^{\infty} dz \int_{-\infty}^{\infty} d^2\boldsymbol{r}_e \int_{-\infty}^{\infty} d^2\boldsymbol{r}'_e \int_0^{\infty} dz_e \int_0^{\infty} dz'_e$$
$$\times e^{i\boldsymbol{k}\cdot(\boldsymbol{r}_e - \boldsymbol{r}'_e)} e^{-|k||2z + z_e + z'_e|}$$
$$\times \psi_i^*(\boldsymbol{r}_e, z_e)\psi_i(\boldsymbol{r}'_e, z'_e)\psi_j(\boldsymbol{r}_e, z_e)\psi_j^*(\boldsymbol{r}'_e, z'_e). \tag{11}$$

The image potential is calculated by integrating with respect to the parallel wave vector up to the cut-off wave number K_c because plasmons exist only for long wavelengths. The integrals in $\boldsymbol{r}_e, \boldsymbol{r}'_e, z$ and $\boldsymbol{k}$ are solved analytically and the part in $z_e z'_e$ and $\boldsymbol{k}_\parallel$ is evaluated numerically. In these calculations the adsorbate wave functions are taken as linear combinations of gaussian orbitals. The procedure of evaluating the integrals is outlined in the appendix.

3. Results and discusion

3.1. Choice of parameters

In a recent paper we reported a model Hamiltonian approach to the CO adsorption on the (110) and (111) surfaces of NiAl (Grillo *et al* 1992). The adsorption was studied in the MOHAAD formalism (Doyen 1976, 1977, Drakova *et al* 1985, 1988). The description of the NiAl(110) metal surface requires input values which were taken from experiments and band structure calculations available in the literature. The choice of these parameters and the corresponding ones for the description of the CO molecule and its interaction with the surface are described elsewhere (Grillo *et al* 1992).

The CO molecule is adsorbed with its molecular axis perpendicular and the C atom closer to the surface. This adsorption geomety has also been established experimentally (Isern 1990). There is strong experimental evidence that CO adsorbs on top of the Ni rows (Isern 1990) as predicted by our previous theoretical investigations. We use this adsorption geometry for the present study of the electron–hole spectra of the CO-covered NiAl(110) surface.

The position of the image plane was found using the same method as was adopted in the static approach (Drakova *et al* 1988) for the evaluation of the image renormalization. In the present work the image plane position needed for the evaluation of the adsorbate–plasmon coupling constants is determined approximately by using the functions $r_{im}(z)$ calculated in the local density approximation (Appelbaum and Hamann 1972).

The parameter r_s needed in the theory is obtained from the experimental bulk plasmon frequency (Mondio *et al* 1991). The expression for the bulk plasmon frequency ω_p of the electron gas is

$$\omega_p = \sqrt{4\pi n}$$

where n is the electronic charge density. It has been used to relate this frequency to r_s. This formula has been generalized (Lucas 1971) to transitions metals of the fifth and sixth period by identifying the effective number of valence electrons per atom

participating in the plasmons from the most stable oxidation state of the metal. The calculated frequencies are in reasonable agreement with the observed energy loss of fast electrons.

The surface cut-off wave vector K_c was obtained from the surface energy σ of NiAl. We use an expression for the surface energy of simple metals, which has already been used before to estimate the long-range correlation part of the surface energy of transition metals (Schmit and Lucas 1972):

$$\sigma = \frac{\sqrt{(2)} - 1}{16\pi}\omega_p K_c^2.$$

The surface energy for NiAl was estimated from the theoretical $r_s^{-5/2}$ dependence. This choice is justified by the work of Schmit and Lucas, which demonstrates that the overall trend of experimental surface energies for transition metals closely follows the same $r_s^{-5/2}$ law as the alkali series (Schmit and Lucas 1972). Although the use of these equations for σ and r_s is based on the nearly-free-electron character of the solid, we may attempt to use these equations as semi-empirical formulae to obtain qualitative information about the plasmon contribution to the surface energy of these materials as has been done by Schmit and Lucas in their plasmon approach to the surface energy of transition metals. The values used for K_c and the energy of the bulk plasmons ω_p in the coupling constant calculation are $K_c = 0.498$ Bohr^{-1} and $\omega_p = 0.755$ Hartree, respectively.

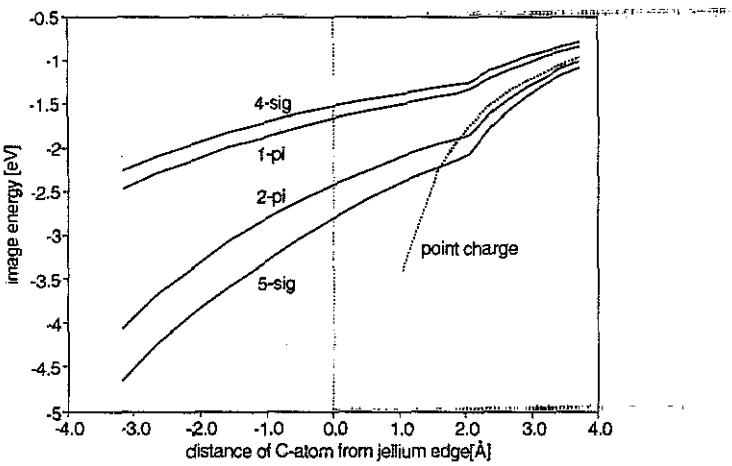

Figure 1. Image potentials of a static unit charge in the unperturbed CO molecular orbitals as a function of the distance z of the C atom from the jellium edge.

3.2. Coupling constants

By using the parameters ω_p and K_c for the adsorbate–plasmon interaction described before, we calculate the coupling constants for the orbital–plasmon interaction. From these coupling constants we can directly obtain the image potentials of a static unit charge in the adsorbate orbitals. Figure 1 shows these image potentials as a function of the distance z of the C atom from the jellium edge for the $1\pi, 2\pi, 4\sigma$ and 5σ

CO orbitals. The comparison to the image potential of a point unit charge localized on the C atom (with the position of the image plane kept fixed at the jellium edge) reveals the influence of the geometrical shape of the adorbitals and the avoidance of the singularity of the classical image potential. The sharp bend in the image potentials at a distance of approximately 2 Å from the jellium edge originates from the variation of the image plane position (Appelbaum and Hamann 1972).

The 5σ orbital has the maximum image potential. This can be explained by the geometry of this orbital as it has the maximum amplitude on the C atom close to the surface. Therefore this orbital induces a strong polarization of the surface plasmons. On the other hand, the 4σ orbital has its maximun amplitude on the O atom which is further away from the surface. For this reason it shows the smallest image potential. The 2π orbital yields relatively large values for the image interaction. This is due to the diffuse character of this orbital. The diffuse cloud of the 2π orbital reaches nearer to the surface as compared to the 1π orbital and this leads to a stronger interaction with the surface plasmons.

The calculation reveals a strong dependence of the image potentials on the shape and the size of the adsorbate orbitals. Including in this way the actual adsorbate charge distribution, a more realistic treatment of the image charge effects is achieved.

3.3. Photoemission spectra

3.3.1. Direct photemission. The selection rules of angle-resolved photoemission (ARUPS) have been used to determine the ionization energies of the 5σ- and 1π-derived chemisorption orbitals (Isern 1990, Mundenar 1987). Under the assumption that the molecular axis of the adsorbed CO molecule is perpendicular to the surface, the polarization dependence of the emission from the two states permitted us to identify their energetic position in the spectrum. The values are given in table 1.

The CO-derived ionization energies for CO adsorbed on NiAl(110) are calculated within the present model Hamiltonian approach. The electron–hole excitation energies are evaluated as differences between the self-consistent ionized states (final states) and the ground state (initial state). In the *static* version of MOHAAD the image effects are included in the initial state. The relaxation of the final state is then solely due to the local adsorbate–metal surface interaction. This approach yields good agreement with the experimental 4σ ionization energy, but the theoretical $4\sigma/5\sigma$ splitting is at variance with the experimental findings which give a larger ionization energy for the 5σ-derived level than for the 1π-derived one. In table 1 the present results are compared to the ionization energies obtained within the static approach and to the experimental values obtained by ARUPS.

Figure 2 displays the calculated spectra (with dynamic image coupling) in comparison to an experimental *angle-integrated* direct and inverse photoemission spectrum. The displayed experimental spectrum does not allow us to identify separately the energies of the 5σ- and 1π-derived emissions, which were derived from different experiments (Isern 1990, Mundenar 1987). The experimental spectra were obtained as the difference between spectra of a CO-covered and a clean surface. The feature of negative intensity, observed in the experimental spectrum in the energy region between the Fermi level and 5 eV below, originates from emission from the d band and can be explained by a change of photoemission matrix elements upon adsorption (Doyen and Ertl 1977).

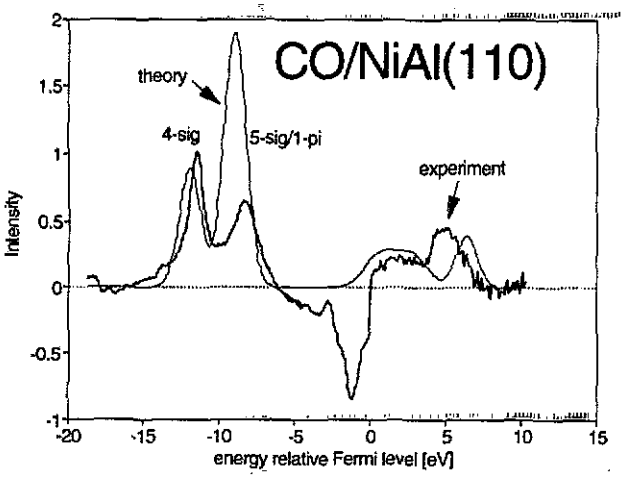

Figure 2. Calculated CO-derived structure in the direct and inverse photoemission spectra for CO adsorbed on NiAl(110) in comparison to the experimental data, which were angle integrated for direct photoemission and at $\bar{\Gamma}$ for inverse photoemission.

The ionization energies of chemisorbed CO are shifted towards the Fermi level relative to the values for gas phase CO. This shift is also present in the experimental direct photoemission spectrum. The calculated 4σ and 5σ ionization energies are in good agreement with the experimental findings. The theoretical 1π ionization energy is at variance with the experiments. This discrepancy is due to the neglect of the 1π–1π electronic repulsion between adjacent co-adsorbed CO molecules in the present calculation, which would reduce the 1π ionization energy considerably.

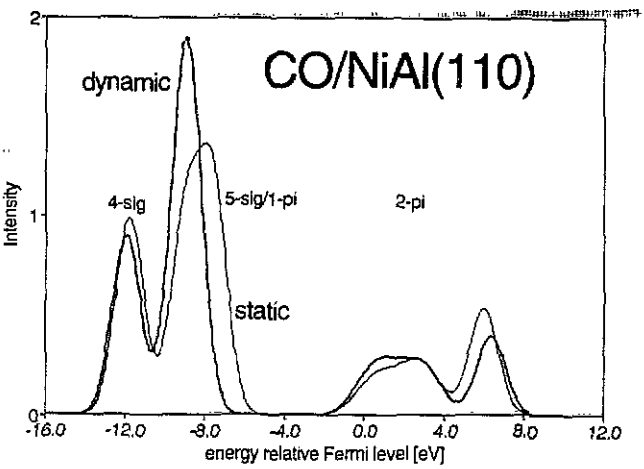

Figure 3. Dynamic and static electron–hole excitation spectra for CO/NiAl(110).

Figure 3 shows the theoretical electron–hole excitation spectra for CO adsorbed on NiAl(110) calculated within the static and the dynamic framework. Compared to the static approach the 5σ ionization energy is shifted to larger binding energies in accordance with the experiments (cf table 1). The reason for this shift is the large image potential of the CO 5σ orbital (cf section 3.2).

We do not include the 6σ CO orbital in our calculations. This can be justified, because this orbital is not involved significantly in the chemisorption bond. However, the image-induced polarization between the 5σ and 6σ orbitals might be of some importance, because they have the same symmetry. Also the image-induced polarization between the 5σ orbital and the sp-metal wave functions is not included at the present stage of our plasmon formalism. Despite these omissions the calculated 5σ ionization potential agrees well with the experimental value. This might indicate that the image-induced polarization does not play too important a role.

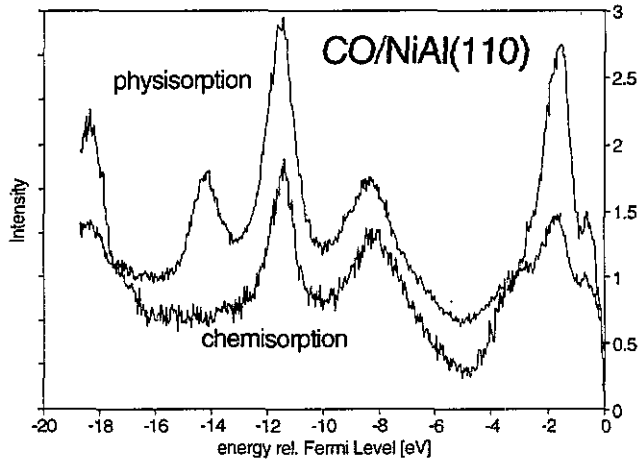

Figure 4. Experimental direct photoemission spectra of chemisorbed CO (lower curve) compared to physisorbed CO on NiAl(110). The energies are given in eV relative to the Fermi level.

In figure 4 the direct photoemission spectra for CO chemisorbed (below) and physisorbed on NiAl(110) are plotted. The physisorption spectrum is characterized by the growing of a third peak at 14.2 eV with respect to the Fermi level (19.3 eV with respect to the vacuum level), which corresponds to the emission from the 4σ-induced hole state. The energy positions of the other two peaks remain unchanged. The ionization energies corresponding to CO physisorbed on NiAl(110) and to CO in the gas phase are shown in table 2.

Table 2. Ionization energies in eV of CO physisorbed on NiAl(110) and in the gas phase.

	Physisorbed CO relative E_{Fermi}	Relative E_{vacuum}	CO gas phase
4σ	14.2	19.3	19.7
1π	11.5	16.6	16.7
5σ	8.4	13.5	14.0

The observed features in the physisorption spectra can be made plausible by our calculations. Comparing the ΔSCF ionization spectra with the CO ionization energies in the gas phase (cf figure 5), it is observed that the 4σ- and $1\pi/5\sigma$-induced features coincide with the 1π and 5σ ionization energies for gas-phase CO, respectively. From this picture the observed change in the direct photoemission

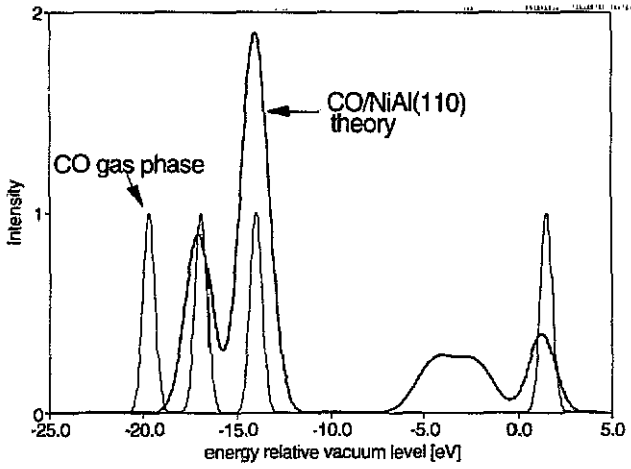

Figure 5. ΔSCF electron–hole excitation spectrum of CO chemisorbed on NiAl(110) compared to CO ionization energies of CO in the gas phase. The energies are given in eV with respect to the vacuum level.

spectrum when physisorbed CO is added to the chemisorption system CO/NiAl(110) might be expected.

3.3.2. Inverse photoemission. The calculated 2π affinity levels are to be compared with inverse photoemission results, which yield the CO-induced features corresponding to the unoccupied levels of the adsorbate system. The two peaks observed above the Fermi level are due to the splitting of the CO 2π orbital in bonding and antibonding levels. This splitting is a consequence of the strong interference between the 2π orbital and the NiAl wave functions above the Fermi level. The energetic position of the calculated bonding level is very similar to the experimental one (cf table 1 and figure 2), whereas the calculated antibonding level is at too large positive energies with respect to the Fermi level when compared to the experimental value. This discrepancy is due to the limitation of the model in describing the unoccupied states of the metal above the vacuum level. These are not taken into account at the present stage in the model of the metal surface. The neglect of these unoccupied metal states causes the observed artificial shift of the antibonding level to too large positive energies.

3.4. Image interaction and relaxation

In order to estimate the importance of the image effects in the relaxation process of the ionized final states, we compare the relaxation energies with the image potential of each CO-induced ion. The relaxation energies are calculated as the energy differences between the Koopmans' and the self-consistent ionization energies. The Koopmans' approximation does not contain any relaxation effect; the final state corresponds to frozen charges in the non-ionized orbitals.

Figure 6 shows the Koopmans' and the self-consistent ionization spectra for CO adsorbed on NiAl(110). The structure in the self-consistent spectrum is shifted to larger binding energies for the unoccupied states above the Fermi level. This is due to the stabilization of the final negative ion through image interaction. The same

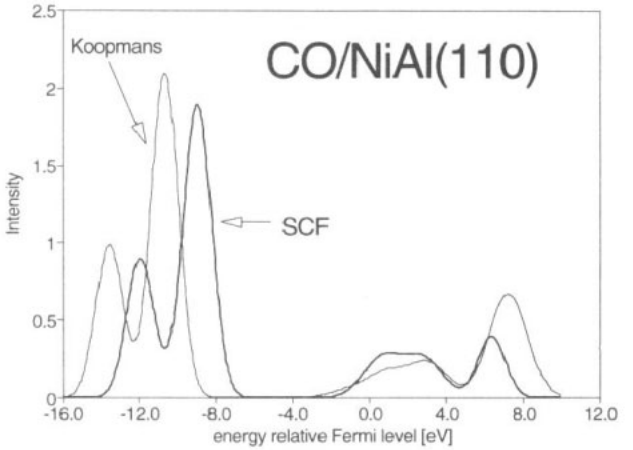

Figure 6. Electron–hole excitation spectra of CO/NiAl(110) in Koopmans' and Δ_{SCF} approximations.

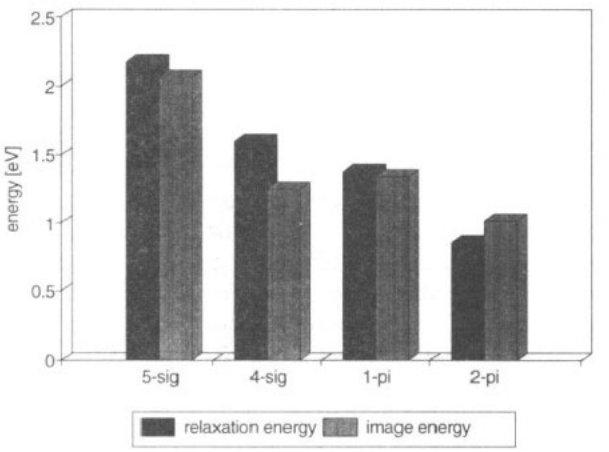

Figure 7. Relaxation energies of CO-derived ionization energies in comparison to image energies for a static charge in an unperturbed CO molecular orbital.

effect is observed for the ionization levels below the Fermi level, leading to smaller ionization energies for the occupied states.

In figure 7 it is observed that the image and the relaxation energies are of the same magnitude for the occupied CO orbitals. This indicates that the image screening effects play an important role in the relaxation mechanism of the final ion. The relaxation shift of the 2π affinity level is considerably smaller than its image potential. This is due to the splitting into 2π bonding and 2π antibonding levels. In this way the population of one 2π affinity level leads only to partial occupation of the unperturbed 2π orbital and therefore induces a smaller relaxation energy than for a completely filled 2π orbital.

The relaxation shifts obtained in the *static* MOHAAD approach are very small compared to those obtained in the present *dynamic* approach (cf table 3). As has already been mentioned (cf section 2.3), relaxation in the static approach occurs

Table 3. Relaxation energies of the molecular orbital hole states of CO/NiAl(110) in the dynamic, ΔRel^{dyn}, and static, ΔRel^{sta}, approaches. The energies are given in eV.

CO orbital	ΔRel^{dyn} (eV)	ΔRel^{sta} (eV)
4σ	1.60	0.13
1π	1.38	0.06
5σ	1.97	0.06

through the local adsorbate–substrate interaction (i.e., interference of wave functions), whereas in the dynamic calculations both processes are contributing to the relaxation shift, namely the local interference effects and the long-range adsorbate–substrate interaction (or image potential screening). The comparison of the two approaches indicates a small contribution of the adsorbate–substrate interference to the relaxation mechanism of the final ionized state. The interplay between the surface plasmon coupling and the hybridization screening has been pointed out before (Gadzuk 1976, 1977, 1979, Gadzuk and Doniach 1978).

4. Conclusions

The theoretical study presented here has led to further insight into the nature of CO adsorption on NiAl alloy. The plasmon theory developed in this work for the treatment of the image force effects in chemisorption provides a useful method for considering the dynamic aspects of the image interaction. The screening charge is determined self-consistently and depends on the geometrical shape of the adorbital charge and the metal surface charge density. The major effect of the image interaction is relaxation of the final ionized state. The effects in the initial state are small. There are no image relaxation effects in the Koopmans' picture. The present investigation shows an important contribution of the image charge interaction to the relaxation mechanism of the final ions for CO adsorbed on a NiAl(110) surface.

The adsorbate–plasmon interaction is described by one- and two-electron operators yielding the change in the electronic motion due to the image interaction. The image-induced polarization of the adsorbate as considered in our dynamical approach is responsible for the Van der Waals forces. The classical limit for the image potential is obtained at large distances from the surface.

The calculated electron–hole excitation spectrum for CO adsorbed on NiAl(110) agrees well with the experimental ionization energies obtained from direct and inverse photoemission spectra. The accuracy of the calculated 5σ ionization energy has been improved with respect to that of the previous static approach due to the larger image potential obtained in the new dynamic approach.

Appendix A. Evaluation of the image potential

This appendix outlines the procedure of evaluating the integral involved in the expression (equation (11)) for the image potential:

$$V_{ij}(r_e, z_e) = \frac{A^2}{\omega_p 2\pi} \int_0^{K_c} dk_x \int_0^{K_c} dk_y \int_0^{\infty} dz \int_{-\infty}^{\infty} d^2 r_e \int_{-\infty}^{\infty} d^2 F r'_e \int_0^{\infty} dz_e \int_0^{\infty} dz'_e$$

$$\times e^{ik\cdot(r_e-r_e')}e^{-|k||2z+z_e+z_e'|}\psi_i^*(r_e,z_e)\psi_i(r_e',z_e')\psi_j(r_e,z_e)\psi_j^*(r_e',z_e')$$
$$= \frac{A^2}{\omega_p 2\pi} I_{ij}(r_e,z_e).$$

Owing to the assumed homogeneous distribution of induced metal dipoles it is convenient to transform the wave vector coordinates parallel to the surface $k_x k_y$ to cylindrical coordinates:

$$d^2k = |k_\parallel|\, dk_\parallel\, d\varphi$$

where $k_\parallel$ is the wave vector parallel to the surface and φ is the angle between this vector and the x-axis. z_e and z_e' are restricted to positive values and therefore the integration over the z-components of the metal dipoles is easily performed. We now rename (r_e, z_e) and (r_e', z_e') as (r, z) and (r_i, z_i), respectively. Then the integral $I_{ij}(r_e, z_e)$ assumes the form:

$$I_{ij} = \frac{1}{2}\int_0^{2\pi} d\varphi \int_0^{K_c} dk_\parallel \int_{-\infty}^{\infty} d^2r \int_{-\infty}^{\infty} d^2r_i \int_0^{\infty} dz \int_0^{\infty} dz_i\, e^{-i|k|\cdot|r-r_i|\cos\varphi}$$
$$\times (1/|k|)e^{-|k|(z+z_i)}\psi_i^*(r,z)\psi_i(r_i,z_i)\psi_j(r,z)\psi_j^*(r_i,z_i). \tag{A1}$$

From now on we write for simplicity $|k| = k$. The φ-dependent part is easily evaluated:

$$I_\varphi = \int_0^{2\pi} d\varphi\, e^{-ik|r-r_i|\cos\varphi} = 2\pi J_0(k|r-r_i|). \tag{A2}$$

Here $J_0(k|r-r_i|)$ is a Bessel function of the first kind (Gradshteyn and Ryzhik 1965). Substituing this in I_{ij} one obtains:

$$I_{ij} = \pi \int_0^{K_c} dk \int_{-\infty}^{\infty} d^2r \int_{-\infty}^{\infty} d^2r_i \int_0^{\infty} dz \int_0^{\infty} dz_i\, J_0(k|r-r_i|)$$
$$\times e^{-k(z+z_i)}\psi_i^*(r,z)\psi_i(r_i,z_i)\psi_j(r,z)\psi_j^*(r_i,z_i). \tag{A3}$$

The Bessel function can be represented by the following infinite series (Arfken 1981):

$$J_0(k|r-r_i|) = \sum_{s=0}^{\infty} \frac{(-1)^s}{s!s!}\left(\frac{1}{2}\right)^{2s} k^{2s}|r-r_i|^{2s}. \tag{A4}$$

By substituing this series in I_{ij} one obtains:

$$I_{ij} = \pi \sum_{s=0}^{\infty}\left(\frac{(-1)^s}{(s!)^2(2)^{2s}}\right)\int_0^{K_c} dk \int_{-\infty}^{\infty} d^2r \int_{-\infty}^{\infty} d^2r_i \int_0^{\infty} dz \int_0^{\infty} dz_i\, k^{2s}|r-r_i|^{2s}$$
$$\times e^{-k(z+z_i)}\psi_i^*(r,z)\psi_i(r_i,z_i)\psi_j(r,z)\psi_j^*(r_i,z_i). \tag{A5}$$

For the sake of briefness we introduce the following compact notation:

$$\Delta r := |r-r_i|$$
$$A_s := \left(\frac{(-1)^s}{(s!)^2(2)^{2s}}\right)$$
$$I_2^s := \int_0^{K_c} dk \int_{-\infty}^{\infty} d^2r \int_{-\infty}^{\infty} d^2r_i \int_0^{\infty} dz \int_0^{\infty} dz_i\, k^{2s}(\Delta r)^{2s}e^{-k(z+z_i)}$$
$$\times \psi_i^*(r,z)\psi_i(r_i,z_i)\psi_j(r,z)\psi_j^*(r_i,z_i).$$

In this way I_{ij} transforms into:

$$I_{ij} = \pi \sum_{s=0}^{\infty} A_s I_2^s.$$

The solution to this integral is found by representing the adsorbate wave function as a linear combination of gaussian orbitals of the form

$$\psi_i(\boldsymbol{r}, z) = \sum_{\alpha}^{n_i} C_g(i, \alpha) g(i, \alpha)$$

where n_i is the number of gaussian components; $g(i, \alpha)$ corresponds to the adsorbate wave function $\psi_i(\boldsymbol{r}, z)$. $C_g(i, \alpha)$ is the coefficient of the αth gaussian given by

$$g(i, \alpha) = A_g(i, \alpha) \mathrm{e}^{-\eta_\alpha^i |\boldsymbol{r} - \boldsymbol{r}_0|^2}$$

where $A_g(i, \alpha)$ is the normalization constant of the gaussian centred at $\boldsymbol{r}_0$ with exponent η_α^i:

$$A_g(i, \alpha) = (2\eta_\alpha^i / \pi)^{3/4}.$$

In this basis I_2^s takes the form

$$I_2^s = \sum_{\alpha}^{n_i} \sum_{\beta}^{n_j} \sum_{\gamma}^{n_i} \sum_{\omega}^{n_j} C_\alpha^i C_\beta^j C_\gamma^i C_\omega^j I_{\alpha\beta\gamma\omega}^s.$$

The integral $I_{\alpha\beta\gamma\omega}^s$ is defined by

$$I_{\alpha\beta\gamma\omega}^s = \int_0^{K_c} \mathrm{d}\boldsymbol{k} \int_{-\infty}^{\infty} \mathrm{d}^2\boldsymbol{r} \int_{-\infty}^{\infty} \mathrm{d}^2\boldsymbol{r}_i \int_0^{\infty} \mathrm{d}z \int_0^{\infty} \mathrm{d}z_i \, k^{2s} (\Delta r)^{2s} \mathrm{e}^{-k(z+z_i)}$$
$$\times \mathrm{e}^{-\eta_\alpha^i |\boldsymbol{r} - \boldsymbol{r}_\alpha|^2} \mathrm{e}^{-\eta_\beta^j |\boldsymbol{r} - \boldsymbol{r}_\beta|^2} \mathrm{e}^{-\eta_\gamma^i |\boldsymbol{r}_i - \boldsymbol{r}_\gamma|^2} \mathrm{e}^{-\eta_\omega^j |\boldsymbol{r}_i - \boldsymbol{r}_\omega|^2}$$

where

$$|\boldsymbol{r} - \boldsymbol{r}_\alpha|^2 = (x - x_\alpha)^2 + (y - y_\alpha)^2 + (z - z_\alpha)^2.$$

The perpendicular and parallel coordinates z and $\boldsymbol{r}$ in $I_{\alpha\beta\gamma\omega}^s$ are separable, so that it is possible to write

$$I_{\alpha\beta\gamma\omega}^s = I^s(k, z, z_i) I^s(\boldsymbol{r}, \boldsymbol{r}_i).$$

In this way I_{ij} can be written as

$$I_{ij} = \pi \sum_{\alpha\beta\gamma\omega}^{n_\alpha n_\beta n_\gamma n_\omega} C_\alpha^i C_\beta^j C_\gamma^i C_\omega^j \sum_{s=0}^{\infty} A_s I^s(k, z, z_i) I^s(\boldsymbol{r}, \boldsymbol{r}_i). \qquad \text{(A6)}$$

The integral $I^s(\boldsymbol{r},\boldsymbol{r}_i)$ is defined by

$$I^s(\boldsymbol{r},\boldsymbol{r}_i)=\sum_{k=0}^{s}\binom{s}{k} I(x,x_i)I(y,y_i) \tag{A7}$$

where $I(x,x_i)$ and $I(y,y_i)$ are given by the following expressions:

$$I(x,x_i)=\mathrm{e}^{-(m+m_i)}\sum_{L=0}^{2(s-k)}(-1)^{2(s-k)-L}\binom{2(s-k)}{L} I_x I_{x_i} \tag{A8}$$

$$I_x=\int_{-\infty}^{\infty}\mathrm{d}x\, x^L \mathrm{e}^{-\eta_{p_1}(x+u)^2}$$

$$I_{x_i}=\int_{-\infty}^{\infty}\mathrm{d}x_i\, x_i^{2(s-k)-L}\mathrm{e}^{-\eta_{p_2}(x_i+u_i)^2}$$

$$I(y,y_i)=\mathrm{e}^{-(N+N_i)}\sum_{L=0}^{2k}(-1)^{2k-L}\binom{2k}{L} I_y I_{y_i} \tag{A9}$$

$$I_y=\int_{-\infty}^{\infty}\mathrm{d}y\, y^L \mathrm{e}^{-\eta_{p_1}(y+u')^2}$$

$$I_{y_i}=\int_{-\infty}^{\infty}\mathrm{d}y_i\, y_i^{2k-L}\mathrm{e}^{-\eta_{p_2}(y_i+u_i')^2}.$$

The constants involved are defined by

$$\begin{aligned}
&\eta_{p_1}=\eta_\alpha^i+\eta_\beta^j\\
&\eta_{p_2}=\eta_\gamma^i+\eta_\omega^j\\
&u=(\Delta x_{\gamma\beta}\eta_\beta-\Delta x_{\alpha\gamma}\eta_\alpha)/\eta_{p_1}\\
&u_i=\Delta x_{\gamma\omega}\eta_\omega/\eta_{p_2}\\
&m=(\eta_\beta\Delta x_{\gamma\beta}^2+\eta_\alpha\Delta x_{\alpha\gamma}^2)-(\Delta x_{\gamma\beta}\eta_\beta-\Delta x_{\alpha\gamma}\eta_\alpha)^2/\eta_{p_1}\\
&m_i=\eta_\omega\Delta x_{\gamma\omega}^2-(\eta_\omega\Delta x_{\gamma\omega})^2/\eta_{p_2}\\
&\Delta x_{\alpha\gamma}=x_\alpha-x_\gamma\\
&\Delta x_{\gamma\beta}=x_\gamma-x_\beta\\
&\Delta x_{\gamma\omega}=x_\gamma-x_\omega\\
&u'=(\Delta y_{\gamma\beta}\eta_\beta-\Delta y_{\alpha\gamma}\eta_\alpha)/\eta_{p_1}\\
&u_i'=\Delta y_{\gamma\omega}\eta_\omega/\eta_{p_2}\\
&N=(\eta_\beta\Delta y_{\gamma\beta}^2+\eta_\alpha\Delta y_{\alpha\gamma}^2)-(\Delta y_{\gamma\beta}\eta_\beta-\Delta y_{\alpha\gamma}\eta_\alpha)^2/\eta_{p_1}\\
&N_i=\eta_\omega\Delta y_{\gamma\omega}^2-(\eta_\omega\Delta y_{\gamma\omega})^2/\eta_{p_2}\\
&\Delta y_{\alpha\gamma}=y_\alpha-y_\gamma\\
&\Delta y_{\gamma\beta}=y_\gamma-y_\beta\\
&\Delta y_{\gamma\omega}=y_\gamma-y_\omega.
\end{aligned}$$

The integrals I_x, I_{x_i}, I_y and I_{y_i} can be evaluated analytically by integrating each variable separately in the following way:

$$I_p = \int_{\infty}^{-\infty} \mathrm{d}p\, p^n \mathrm{e}^{-\eta_p(p+v)^2} = \frac{\mathrm{e}^{-\eta p v^2}}{\sqrt{\eta_p}^{n+1}} I_m^n$$

$$I_m^n = \frac{1}{2^{n-1}}\sqrt{\pi}\frac{\mathrm{d}^{n-1}}{\mathrm{d}(q)}(q\mathrm{e}^{q^2})$$

where

$$p = x, x_i, y, y_i$$
$$q = -\sqrt{\eta_p}v$$
$$n = 0, 1 \ldots, 2s.$$

For each term in the sum over s in equation (A6) $2s$ integrals of the above kind have to be calculated.

The integral $I^s(k, z, z_i)$ has the form

$$I^s(k, z, z_i) = \frac{\pi}{4\sqrt{\eta_{p_1}\eta_{p_2}}}\int_0^{K_c} k^{2s}\mathrm{e}^{(k^2L_2 - kL_3 - L_1)} \times \mathrm{Erf}(\sqrt{\eta_{p_1}}a_k)\mathrm{Erf}(\sqrt{\eta_{p2}}a'_k). \tag{A10}$$

The error functions $\mathrm{Erf}(\sqrt{\eta_{p1}}a_k)$ and $\mathrm{Erf}(\sqrt{\eta_{p2}}a'_k)$ were calculated numerically. They are defined by

$$\mathrm{Erf}(\sqrt{\eta_{p1}}a_k) = \frac{2}{\sqrt{\pi}}\int_{\sqrt{\eta_{p1}}a_k}^{\infty} \mathrm{e}^{-u^2}\mathrm{d}u$$

with

$$a_k = [k - 2(\eta_\alpha z_\alpha + \eta_\beta z_\beta)]/2\eta_{p1}$$
$$a'_k = [k - 2(\eta_\gamma z_\gamma + \eta_\omega z_\omega)]/2\eta_{p2}$$
$$L_1 = [z_\alpha^2\eta_\alpha(1 - \eta_\alpha/\eta_{p1}) + z_\beta^2\eta_\beta(1 - \eta_\beta/\eta_{p1}) - 2\eta_\alpha\eta_\beta z_\alpha z_\beta/\eta_{p1}] + [z_\gamma^2\eta_\gamma(1 - \eta_\gamma/\eta_{p2}) + z_\omega^2\eta_\omega(1 - \eta_\omega/\eta_{p2}) - 2\eta_\gamma\eta_\omega z_\gamma z_\omega/\eta_{p2}]$$
$$L_2 = \tfrac{1}{4}(1/\eta_{p1})(1/\eta_{p2})$$
$$L_3 = (\eta_\alpha z_\alpha + \eta_\beta z_\beta)/\eta_{p1} + (\eta_\gamma z_\gamma + \eta_\omega z_\omega)/\eta_{p2}$$
$$u = \sqrt{\eta_{p1}}(z + a_k)$$
$$u_i = \sqrt{\eta_{p2}}(z_i + a'_k).$$

Summarizing the final expression for the image potential yields

$$V_{ij}(r_e, z_e) = \frac{1}{2\pi}I_{ij}(r_e, z_e).$$

Here $I_{ij}(r_e, z_e)$ is defined by equations (A6), (A7) and (A10). The constant A in V_{ij} was set equal to $\sqrt{\omega_p}$ yielding the classical limit for a point charge at large distances from the surface $V_{ij}(z) \to 1/4z$.

Acknowledgments

Financial support by the Sonderforschungsbereich 6, by the Fonds der Chemischen Industrie and by the Deutscher Akademischer Austauschdienst is gratefully acknowledged. The authors are indebted to Dejana Drakova for assistance and helpful discussions. M E Grillo wishes to express her gratitude to the theoretical group of Matthias Scheffler at the Fritz-Haber-Institut in Berlin for its hospitality and financial support.

References

Anda E, Majlis N and Grempel D 1977 *J. Phys. C: Solid State Phys.* **10** 2365–82
Anda E and Ure J E 1979 *Surf. Sci.* **83** 572–84
Appelbaum J A and Hamann D R 1972 *Phys. Rev.* B **6** 1122–30
Arfken G 1981 *Mathematical Methods for Physicists* (New York: Academic) p 551
Braun O M and Volokitin A I 1983 *Surf. Sci.* **131** 148–58
Cini M 1978 *Phys. Rev.* B **17** 2486–93
—— 1979 *Surf. Sci.* **79** 589–607
Doyen G 1976 *Surf. Sci.* **59** 461–87
Doyen G and Ertl G 1977 *Surf. Sci.* **65** 641–67
—— 1977 *Surf. Sci.* **69** 157–84
—— 1977 *Proc. 7th Int. Vac. Congr. and 3rd Int. Conf. on Solid Surfaces (Vienna, Austria)* p 703–6
Drakova D, Doyen G and Hübner R 1988 *J. Chem. Phys.* **89** 1725–40
Drakova D, Doyen G and von Trentini F 1985 *Phys. Rev.* B **32** 6399–423
Dunlap B I and Gadzuk J W 1980 *Surf. Sci.* **94** 89–104
Franklin J L, Dillard J G, Rosenstick H M, Herron J T, Draxl K and Field F H 1969 Ionization potentials, appearance potentials and heats of formation of gaseous ions *Report No* NSRDS-NBS 26 (Washington, DC)
Gadzuk J W 1967 *Surf. Sci.* **6** 133–58
—— 1976 *Phys. Rev.* B **14** 2267–80
—— 1977 *Surf. Sci.* **67** 77–88
—— 1979 *Surf. Sci.* **86** 516–28
Gadzuk J W and Doniach S 1978 *Surf. Sci.* **77** 427–48
Gerlach E 1971 *Phys. Rev.* B **4** 393–6
Gradshteyn I S and Ryzhik I M 1965 *Table of Integrals, Series and Products* (New York: Academic) p 482
Grillo M E 1991 *PhD Thesis* Universidad Central de Venezuela
Grillo M E, Castro G R and Doyen G 1992 *J. Chem. Phys.* submitted
Heskett D, Plummer EW and Messmer R P 1984 *Surf. Sci.* **139** 558–68
Hewson A C and Newns D M 1974 *Japan. J. Appl. Phys. Suppl.* 2 121–30
Isérn H 1990 *PhD Thesis* Universidad Central de Venezuela
Janak J F, Williams A R and Moruzzi V L 1975 *Phys. Rev.* B **11** 1522–36
Kahn L M and Ying S C 1976 *Surf. Sci.* **59** 333–60
Lang N D and Kohn W 1973 *Phys. Rev.* B **7** 3541–50
Löwdin P-O 1950 *J. Chem. Phys.* **18** 365–75
Lucas A A 1971 *Phys. Rev.* B **4** 2939–49
Mahan G D 1972 *Phys. Rev.* B **5** 739–44
Mondio G, Nery F, Stoecker M, Janssens T, Castro G R and Wandelt K 1991 *Surf. Sci.* **251** 243–7
Mundenar J M 1987 *PhD Thesis* University of Pennsylvania
Mundenar J M, Gaylord R H, Lui S C, Plummer E W, Zehner D M, Ford W K and Sneddon L G 1987 *Mater. Res. Soc.* **83** 59–66
Remy M 1970 *J. Chem. Phys.* **53** 2487–91
Ritchie R H 1972 *Phys. Lett.* **38A** 189–90
Ritchie R H and Wilems R E 1969 *Phys. Rev.* **178** 372–81
Russier V and Mijoule C 1991 *Phys. Rev.* B **44** 3970–80

Schmit J and Lucas A A 1972 *Solid State Commun.* **11** 419–22
Sunjic M, Toulouse G and Lucas A A 1972 *Solid State Commun.* **11** 1629–31
Tracy J C 1972 *J. Chem. Phys.* **56** 2748–54